Heriot-Watt University

Wavelength scaling of terahertz generation by gas ionization

Clerici, Matteo; Peccianti, Marco; Schmidt, Bruno E; Caspani, Lucia; Shalaby, Mostafa; Giguère, Mathieu; Lotti, Antonio; Couairon, Arnaud; Légaré, François; Ozaki, Tsuneyuki; Faccio, Daniele Franco Angelo; Morandotti, Roberto

Wavelength Scaling of Terahertz Generation by Gas Ionization

Matteo Clerici,[1,2,*] Marco Peccianti,[3,1] Bruno E. Schmidt,[1] Lucia Caspani,[1] Mostafa Shalaby,[1] Mathieu Giguère,[1]
Antonio Lotti,[4,5] Arnaud Couairon,[5] François Légaré,[1] Tsuneyuki Ozaki,[1] Daniele Faccio,[2,†] and Roberto Morandotti[1]

[1]*INRS-EMT, 1650 Boulevard Lionel-Boulet, Varennes, Québec J3X 1S2, Canada*
[2]*School of Engineering and Physical Sciences, Heriot-Watt University, SUPA, Edinburgh EH14 4AS, United Kingdom*
[3]*Institute for Complex Systems (ISC), CNR, via dei Taurini 19, 00185 Rome, Italy*
[4]*Dipartimento di Scienza e Alta Tecnologia, Università degli Studi dell'Insubria, via Valleggio 11, 22100 Como, Italy*
[5]*Centre de Physique Théorique CNRS, École Polytechnique, F-91128 Palaiseau, France*
(Received 24 January 2013; published 17 June 2013)

Low-frequency currents induced by ultrashort laser-driven ionization can emit extremely broadband, single-cycle terahertz pulses. We present a model that predicts a strong wavelength dependence of the THz emission in good agreement with our experimental study. This reveals that the combined effects of plasma currents rising proportionally to the square of the pump wavelength and wavelength-dependent focusing conditions lead to 30 times higher THz emission at 1800 nm compared to an 800 nm wavelength. Unrivaled single-cycle electric field strengths of 4.4 MV/cm are achieved with this compact table-top setup.

High-field terahertz (THz) pulses with frequencies in the 1–10 THz region are of enormous interest for a variety of applications ranging from standoff THz spectroscopy to novel nonlinear THz interactions, e.g., in graphene or other media. However, currently high-field THz pulses (peak field $\simeq 20$ MV/cm) can only be provided by large-scale, accelerator-based facilities [1], whereas table-top solutions (relying on small-scale laser systems) are still an open issue, which is mainly being addressed by optical rectification in nonlinear crystals, resulting in peak fields currently limited to $\simeq 1.5$ MV/cm [2,3]. Higher field values can be achieved by difference-frequency generation in second-order nonlinear crystals but are limited to the >10 THz carrier frequency regime [4,5]. Laser-induced ionization in symmetry-broken laser fields, obtained by focusing an optical pulse together with its second harmonic in a gas [6], may provide a viable solution for high-field table-top THz generation owing to the extremely large bandwidths and remarkable focusing properties of the generated pulses [7,8], an important feature that allowed Bartel and coworkers to report peak field values up to 0.5 MV/cm [9].

However, until now, attempts to further increase the THz peak field have essentially relied on increasing the pump energy. Unfortunately this method is hampered, on the one hand by saturation effects due to plasma defocusing as well as other detrimental nonlinear mechanisms that act to finally quench the increase of the THz generation efficiency [10,11] currently limited to 10^{-4}–10^{-5} [12,13]. On the other hand, increasing the radiated THz energy does not necessarily translate to higher THz peak fields since the spatial and temporal profiles as well as the coherence properties of the optical pump play a role in determining the spatial and temporal properties of the THz field [11,14]. No methods to significantly scale up the THz generation

efficiency or peak field in plasma have proven to be effective so far.

In this Letter, we demonstrate an effective wavelength scaling mechanism for single-cycle THz field generation. Our approach is inspired by a similar paradigm-changing demonstration at the opposite end of the electromagnetic spectrum, i.e., soft x-ray or extreme ultraviolet (XUV) generation by laser-induced tunneling processes in gases [15]. Remarkable photon yields in the x-ray water window have been demonstrated by pumping with longer laser wavelengths in order to take advantage of the wavelength λ^2 scaling of the laser-induced ponderomotive energy (see, e.g., Ref. [16]). Although the physics of THz generation is different from XUV generation, similar scaling laws in the intensity of the laser-induced plasma currents (and hence THz emission) have also been studied numerically following our preliminary theoretical and experimental results [17,18]. Our model verified by experimental results shows an effective wavelength scaling mechanism proportional to $\lambda^{4.6}$ for single-cycle THz field generation by two-color laser-induced ionization. It also indicates the possibility of a further scaling at longer wavelengths.

We first describe THz generation from a two-color laser-induced plasma filament generalized in order to account for the effect of wavelength scaling and also of the specific focusing conditions (i.e., plasma filament volume) that are achieved in our experiments. Modeling the photocurrent mechanism requires solving the equations that describe the evolution of the current source for THz generation driven by the laser field [11,19]

$$\frac{\partial J_x}{\partial t} + \frac{J_x}{\tau_c} = \frac{e^2}{m_e} N_e E_x - \frac{e}{m_e} \frac{J_z}{c} E_x, \tag{1a}$$

$$\frac{\partial J_z}{\partial t} + \frac{J_z}{\tau_c} = \frac{e}{m_e} \frac{J_x}{c} E_x, \tag{1b}$$

where e, m_e, and N_e denote the electron charge, mass, and density, while τ_c is the collision time. E_x represents the two-color driving laser field, linearly polarized and propagating along z; J_x and J_z indicate the two components of the electron current density perpendicular and parallel to the laser pulse propagation direction, respectively. We note that Eqs. (1a) and (1b) include both the effect of the laser pulse electric field and the effect of the magnetic Lorentz force expressed by the last term on the right-hand sides of each equation. We assume that N_e is generated by optical field ionization (rather than by electron collisions). This process involves the evolution equation for electron production by field ionization from the density $N_{A,M}(r, z, t)$ of the neutral atoms (A) or molecules (M): $\partial N_{A,M}/\partial t = -W(|E|)N_{A,M}$, from which the electron density $N_e(r, z, t)$ is obtained by charge conservation. The field-dependent ionization rate $W(|E|)$ follows the Keldysh formulation [20] (see details in Ref. [21]). We note that in the tunneling regime, the ionization rates do not depend on the wavelength. The model we are considering is, however, valid from the multiphoton to the tunneling regime and includes a wavelength dependence in the domain of intensities corresponding to multiphoton ionization. We take the polarization of the second harmonic field, also propagating in the z direction, to be parallel to the polarization of the fundamental pulse and the complete two-color laser field is included as a single component: $E_x = E_\omega + E_{2\omega}$. To first approximation, the collision time τ_c is much longer than the optical period, and the currents can be obtained as a power expansion of the pump electric field:

$$J_x^{(1)} \propto \frac{e^2}{\omega m_e} N_e E_x. \qquad (2)$$

The photocurrent term in Eq. (2) is dominant for THz generation in the two-color configuration, provided that the relative phase between the fundamental and the second harmonic fields ensures the required asymmetry in the ionization [11,19], e.g., when the phase difference between fundamental and second harmonic approaches π. Equation (2) predicts, in the case of tunneling ionization, a linear dependence of the transverse photocurrent from the pump wavelength, which in turn results in a quadratic scaling of the radiated THz energy with the pump wavelength, i.e., as λ^2, for a wavelength-independent excitation volume (see also the Supplemental Material [22]).

In order to correctly model an experiment, we then need to carefully account for the specific focusing conditions adopted when comparing the THz yield with varying pump wavelengths. For example, in this work we choose to use both a fixed focal length input focusing mirror and a fixed input energy. This results in a beam focusing volume and peak pump intensity that will change with wavelength as a result of simple linear focusing considerations. In more detail, for fixed focusing and input energy conditions the plasma length and radius (determined by the focused

Gaussian beam Rayleigh range and diameter, respectively) scale as λ, while the peak intensity decreases as λ^{-2}. Including these parameters in the numerical simulation will therefore introduce a correction to the simple THz energy λ^2 scaling law predicted above. The precise impact of all these parameters is determined by numerically evaluating the THz emission and calculating the macroscopic photocurrent source term considering a 60 fs pulse duration, 400 μJ input pulse energy, and a 20 μJ second harmonic energy for varying wavelengths between 0.8 and 2 μm. For simplicity, the plasma density has been considered uniform over the linearly focused beam Rayleigh range. The radiated THz energy is then obtained by integrating the photocurrent source term over the effective volume, as described in the Supplemental Material [22]. The solid line in Fig. 1(a) depicts the results of this model: a remarkable wavelength scaling is predicted that is actually much larger than $\sim \lambda^2$ and is the combined result of both the fundamental λ^2 law resulting from the actual plasma currents and the effect of the wavelength-dependent plasma volume. However, we note how the model also predicts a sudden drop in the THz conversion
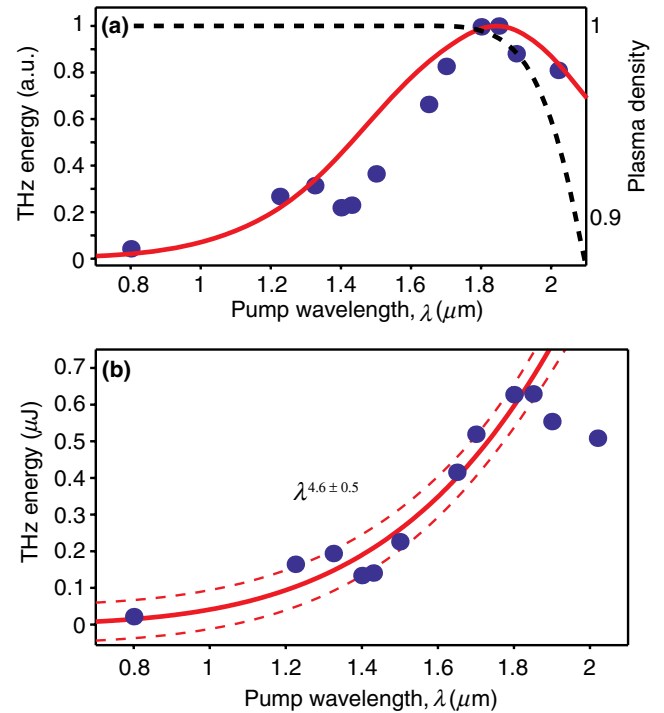

FIG. 1 (color online).   (a) Radiated THz energy dependence on the pump laser wavelength obtained by numerical integration of the transverse photocurrent model for different pump wavelengths (red solid curve). The black dashed curve shows the calculated plasma density (right axis). The energy scale in (a) is normalized and the experimental data are overlapped for clarity (solid circles). (b) Recorded THz energy for 12 different pump wavelengths between 0.8 and 2.02 μm (solid circles). The red solid curve shows the power law fit ($\lambda^{4.6\pm0.5}$) together with the 65% confidence bounds (red dashed curves).

efficiency for wavelengths longer than 1.8 μm. This drop is to be attributed to the fact that with increasing wavelength (and all other fixed input conditions as described above), the peak intensity decreases. For shorter wavelengths, the medium is completely ionized, $N = 1$. However, at $\lambda \sim 1.8$ μm the threshold is reached for which ionization drops below 100% [black dashed curve in Fig. 1(a)]. Consequently, the associated THz emission suffers a sudden drop. This indicates a clear feature in the THz yield that is related only to the specific focusing conditions adopted in this work and at the same time indicates a route to maintaining the THz wavelength scaling, i.e., by controlling the input conditions in a different fashion.

In our experiments, carried out at the infrared beam line of the advanced laser light source (ALLS) [23], we considered the same parameters and conditions used in the model. The layout is sketched in Fig. 2: we employed 12 different pump wavelengths for the THz generation between 800 nm and 2.02 μm. The 1.225–2.02 μm pulses were delivered by a commercial optical parametric amplifier (TOPAS, Light Conversion Ltd.), while the 800 nm pulse came directly from the laser amplifier. The pulse duration was 60 ± 5 fs (full width at half maximum) throughout all the measurements and was monitored using a home-built frequency resolved optical gating. We also fixed the focusing condition: $\simeq 6$ mm beam waist (after spatial mode cleaning in a vacuum cell) collimated on a 4 in. equivalent focal length (EFL), 90 deg off-axis parabolic mirror. A free-standing, 100 μm thick β-barium borate (BBO) crystal was employed for frequency doubling the pump pulses, and all the measurements have been performed for a fixed fundamental to second harmonic energy ratio of $\simeq 5\%$ while the BBO-plasma distance was also fixed at $\simeq 1.2$ cm. The setup was purged with pure
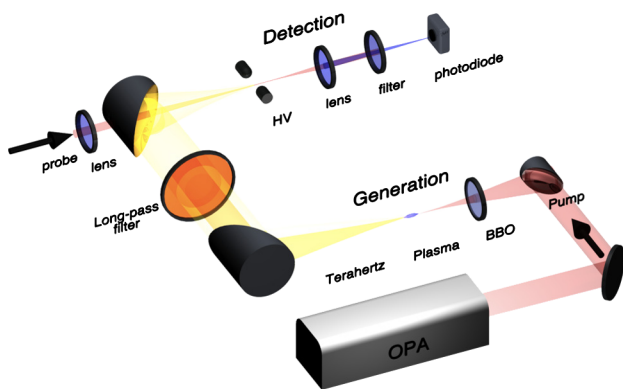

FIG. 2 (color online). The wavelength tunable output from a commercial optical parametric amplifier (OPA) is focused together with its second harmonic generated by a BBO crystal. The generated THz pulse is collected by a parabolic imaging system and focused into the detection setup. The time-resolved electric field is detected via ABCD. A pyroelectric detector and a camera also monitor pulse energies and beam profiles, respectively.

nitrogen so as to avoid THz absorption from atmospheric water molecules. Finally, the input fundamental pulse energy was fixed at 400 ± 5 μJ. For all wavelengths, the total THz energy radiated from the few-millimeter-long plasma source was measured by a calibrated, commercial pyroelectric detector (Molectron, Coherent) after eliminating the pump radiation with three long-pass multimesh filters (QMC Instruments Ltd.) providing 10^{-6} total rejection above 20 THz. Figure 1(b) shows the radiated THz energy as a function of increasing pump wavelength [solid circles, also shown in Fig. 1(a)]. In particular, we can highlight a clear monotonic increase in the THz yield fitted by a $\lambda^{4.6 \pm 0.5}$ power law in Fig. 1(b), which continues up to pump wavelengths of 1.8 μm. Pump wavelengths longer than $\simeq 1.85$ μm show an actual decrease in the observed THz energy and conversion efficiency, in very good agreement with our model. In the reported data, the maximum gain in the energy conversion efficiency calculated as the ratio between the THz energy at 1.85 μm and at 0.8 μm (i.e., the standard pump wavelength used in all experiments to date) reaches up to a factor of 30.

In order to fully characterize the generated THz pulses, we recorded both their electric field and beam profile. For the time-resolved electric field measurement, we relied on the air-biased-coherent-detection scheme (ABCD) [24,25] performed via a 45 fs (full width at half maximum), 800 nm, 40 μJ probe pulse focused to a $\simeq 10$ μm spot size. The probe pulse was overlapped to the THz beam tightly focused by a 90 deg off-axis parabolic mirror (2 in. EFL, 2 in. aperture, see Fig. 2) via a 1.5 mm diameter hole in the mirror. An oscillating electric field of (26.7 ± 2) kV/cm biased the interaction, and the signal was detected after suitable filtering by an amplified photodiode (Femtowatt, New Focus) and a lock-in amplifier. Figure 3 shows the normalized THz field temporal profiles [Fig. 3(a)] and relative power spectra [Fig. 3(b)] for an 800, 1450, and 1850 nm pump laser pulse wavelength. The electric fields and spectra are relatively similar in shape, confirming that we scale the THz energy while maintaining the temporal quality of the single-cycle THz electric field pulse. In addition, we recorded with a camera (PV-320, Electrophysics) the THz beam profile generated by the 1850 nm pump pulse at the detection plane, replacing the last THz focusing mirrors with a 2 in. EFL mirror without a hole. The sub-90 μm THz beam shown in Fig. 3(c) proves that the generated THz field is characterized by an excellent—near wavelength-limited—focusability.

The THz electric field for a 1850 nm pump pulse has been evaluated considering the recorded energy $U = (630 \pm 15)$ nJ, the temporal THz electric field trace $E_m(t)$, and the beam profile obtained via a Gaussian fit of the recorded data: $\mathcal{G}(x, y) = \exp(-x^2/\sigma_x^2 - y^2/\sigma_y^2)$ with $\sigma_x = (89 \pm 3)$ μm and $\sigma_y = (82 \pm 4)$ μm. Considering $\mathcal{E}_m(t)$ such that $E_m(t) = \Re[\mathcal{E}_m(t)]$ and η_0 the vacuum impedance (377 Ω), the THz field reads
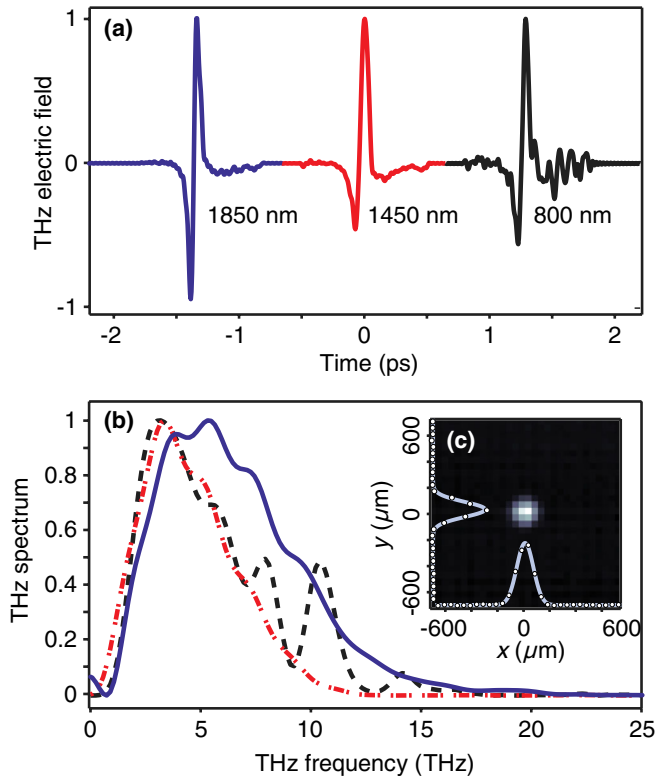
FIG. 3 (color online).   (a) Normalized THz electric field traces acquired by the ABCD detection scheme for a 400 μJ pump energy at 1850, 1450, and 800 nm pump wavelengths (left to right, shifted in time for visualization purposes). (b) Power spectra of the THz fields in panel (a) (800 nm dashed, 1450 nm dot dashed, and 1850 nm solid). (c) THz beam profile recorded in the focus of the last parabolic mirror for the 1850 nm pump wavelength. The overlay in (c) shows the Gaussian fit for the THz spot size in the parabolic focus.

$$E(t) = \frac{E_m(t)}{\max(|\mathcal{E}_m(t)|)} \sqrt{\frac{2\eta_0 U}{\int dx dy \, \mathcal{G}(x,y) \int dt \frac{|\mathcal{E}_m(t)|^2}{\max(|\mathcal{E}_m(t)|^2)}}},$$

and the field amplitude generated by the 1850 nm pump pulse reaches what is, to the best of our knowledge, the highest reported value for a single-cycle sub-10 THz pulse delivered by a table-top source: 4.4 ± 0.4 MV/cm.

The excellent agreement between our model and the experimental data allows us to speculate that the main wavelength-scaling effects at play are related to the photocurrent amplitudes combined with linear focusing geometry effects. This suggests that under the appropriate focusing conditions, e.g., for constant intensity and interaction volume, it would be possible to further increase the THz energy with pump wavelengths longer than 2 μm (see comments in the Supplemental Material [22]).

We note that alternative wavelength scaling mechanisms may arise either due to higher-order (e.g., ponderomotive [26]) terms in the plasma currents or from an enhanced ionization asymmetry induced by single-cycle dynamics [27]. Both these effects have been predicted for single-color

laser driving schemes, where waveform controlled THz generation has been recently demonstrated by means of midinfrared few-cycle pulses [28]. These mechanisms, however, typically have conversion efficiencies orders of magnitude lower than those observed here [19] (see Supplemental Material [22] for a detailed discussion).

In conclusion, we show that scaling to longer wavelengths strongly boosts the down-conversion efficiency in the THz region. The agreement between our model and the experiments indicate that the dominant scaling mechanism is related to the induced plasma currents but also shows a strong dependence on the input focusing conditions. We observe the generation of linearly polarized THz pulses with conversion efficiencies from the midinfrared pump to the THz pulse $>10^{-3}$, i.e., almost 2 orders of magnitude higher than in previous plasma-based generation experiments performed with an 800 nm pump wavelength at similar laser pump energies, featured by a record-breaking THz peak field (4.4 MV/cm). We envisage that scaling further with longer wavelengths is certainly feasible and will pave the way for applications in nonlinear THz optics. As a first example, we note that our source allowed us to discover a novel counterpropagating nonlinear wave-mixing effect in diamond [29], 3D space-time mapping of THz fields by means of standard CCD [30], and THz-triggered coherent emission from excited nitrogen molecules, which will be described elsewhere.

*clerici@emt.inrs.ca
†d.faccio@hw.ac.uk

[1] D. Daranciang, J. Goodfellow, M. Fuchs, H. Wen, S. Ghimire, D. A. Reis, H. Loos, A. S. Fisher, and A. M. Lindenberg, Appl. Phys. Lett. **99**, 141117 (2011).

[2] H. Hirori, A. Doi, F. Blanchard, and K. Tanaka, Appl. Phys. Lett. **98**, 091106 (2011).

[3] C. P. Hauri, C. Ruchert, C. Vicario, and F. Ardana, Appl. Phys. Lett. **99**, 161116 (2011).

[4] A. Sell, A. Leitenstorfer, and R. Huber, Opt. Lett. **33**, 2767 (2008).

[5] F. Junginger, A. Sell, O. Schubert, B. Mayer, D. Brida, M. Marangoni, G. Cerullo, A. Leitenstorfer, and R. Huber, Opt. Lett. **35,** 2645 (2010).

[6] D. J. Cook and R. M. Hochstrasser, Opt. Lett. **25,** 1210 (2000).

[7] K. Y. Kim, A. J. Taylor, J. H. Glownia, and G. Rodriguez, Nat. Photonics **2,** 605 (2008).

[8] M. D. Thomson, V. Blank, and H. G. Roskos, Opt. Express **18,** 23 173 (2010).

[9] T. Bartel, P. Gaal, K. Reimann, M. Woerner, and T. Elsaesser, Opt. Lett. **30,** 2805 (2005).

[10] M. D. Thomson, M. Kreß, T. Löffler, and H. G. Roskos, Laser Photonics Rev. **1,** 349 (2007).

[11] K.-Y. Kim, J. H. Glownia, A. J. Taylor, and G. Rodriguez, Opt. Express **15,** 4577 (2007).

[12] T.-J. Wang, Y. Chen, C. Marceau, F. Theberge, M. Châteauneuf, J. Dubois, and S. L. Chin, Appl. Phys. Lett. **95,** 131108 (2009).

[13] G. Rodriguez and G. L. Dakovski, Opt. Express **18,** 15 130 (2010).

[14] I. Babushkin, W. Kuehn, C. Köhler, S. Skupin, L. Bergé, K. Reimann, M. Woerner, J. Herrmann, and T. Elsaesser, Phys. Rev. Lett. **105,** 053903 (2010).

[15] F. Krausz and M. Ivanov, Rev. Mod. Phys. **81,** 163 (2009).

[16] T. Popmintchev, M.-C. Chen, D. Popmintchev, P. Arpin, S. Brown, S. Alisauskas, G. Andriukaitis, T. Balciunas, O. Mucke, A. Pugzlys, A. Baltuska, B. Shim, S. Schrauth, A. Gaeta, C. Hernandez-Garcia, L. Plaja, A. Becker, A. Jaron-Becker, M. Murnane, and H. Kapteyn, Science **336,** 1287 (2012).

[17] M. Clerici, M. Peccianti, B. Schmidt, L. Caspani, M. Shalaby, M. Giguère, A. Lotti, A. Couairon, F. Légaré, T. Ozaki, D. Faccio, and R. Morandotti, arXiv:1207.4754.

[18] L. Bergé, S. Skupin, C. Kohler, I. Babushkin, and J. Herrmann, Phys. Rev. Lett. **110,** 073901 (2013).

[19] A. V. Balakin, A. V. Borodin, I. A. Kotelnikov, and A. P. Shkurinov, J. Opt. Soc. Am. B **27,** 16 (2009).

[20] L. V. Keldysh, Sov. Phys. JETP **20,** 1307 (1965).

[21] A. Couairon and A. Mysyrowicz, Phys. Rep. **441,** 47 (2007).

[22] See Supplemental Material at http://link.aps.org/supplemental/10.1103/PhysRevLett.110.253901 for details on the model and on the wavelength dependence of the different terms accounting for the radiated THz energy.

[23] B. E. Schmidt, A. D. Shiner, M. Giguère, P. Lassonde, C. A. Trallero-Herrero, J.-C. Kieffer, P. B. Corkum, D. M. Villeneuve, and F. Légaré, J. Phys. B **45,** 074008 (2012).

[24] J. Dai, X. Xie, and X.-C. Zhang, Phys. Rev. Lett. **97,** 103903 (2006).

[25] N. Karpowicz, J. Dai, X. Lu, Y. Chen, M. Yamaguchi, H. Zhao, X.-C. Zhang, L. Zhang, C. Zhang, M. Price-Gallagher, C. Fletcher, O. Mamer, A. Lesimple, and K. Johnson, Appl. Phys. Lett. **92,** 011131 (2008).

[26] J. Peñano, P. Sprangle, B. Hafizi, D. Gordon, and P. Serafim, Phys. Rev. E **81,** 026407 (2010).

[27] W.-M. Wang, S. Kawata, Z.-M. Sheng, Y.-T. Li, L.-M. Chen, L.-J. Qian, and J. Zhang, Opt. Lett. **36,** 2608 (2011).

[28] Y. Bai, L. Song, R. Xu, C. Li, P. Liu, Z. Zeng, Z. Zhang, H. Lu, R. Li, and Z. Xu, Phys. Rev. Lett. **108,** 255004 (2012).

[29] M. Clerici, L. Caspani, E. Rubino, M. Peccianti, M. Cassataro, A. Busacca, T. Ozaki, D. Faccio, and R. Morandotti, Opt. Lett. **38,** 178 (2013).

[30] M. Clerici, D. Faccio, L. Caspani, M. Peccianti, E. Rubino, L. Razzari, F. Légaré, T. Ozaki, and R. Morandotti, Opt. Lett. **38,** 1899 (2013).